

PUAL: A Classifier on Trifurcate Positive-Unlabeled Data

Xiaoke Wang¹, Xiaochen Yang², Rui Zhu^{3*}, Jing-Hao Xue¹

¹Department of Statistical Science, University College London, Gower Street, London, WC1E 6BT, England, UK.

²School of Mathematics & Statistics, University of Glasgow, University Place, Glasgow, G12 8QQ, Scotland, UK.

^{3*}Bayes Business School, City, University of London, 106 Bunhill Row, London, EC1Y 8TZ, England, UK.

*Corresponding author(s). E-mail(s): rui.zhu@city.ac.uk;
Contributing authors: xiaoke.wang.18@ucl.ac.uk;
xiaochen.yang@glasgow.ac.uk; jinghao.xue@ucl.ac.uk;

Abstract: Positive-unlabeled (PU) learning aims to train a classifier using the data containing only labeled-positive instances and unlabeled instances. However, existing PU learning methods are generally hard to achieve satisfactory performance on trifurcate data, where the positive instances distribute on both sides of the negative instances. To address this issue, firstly we propose a PU classifier with asymmetric loss (PUAL), by introducing a structure of asymmetric loss on positive instances into the objective function of the global and local learning classifier. Then we develop a kernel-based algorithm to enable PUAL to obtain non-linear decision boundary. We show that, through experiments on both simulated and real-world datasets, PUAL can achieve satisfactory classification on trifurcate data.

1 Introduction

PU learning is to train a classifier from PU data, which only contain labeled-positive instances and unlabeled instances, i.e., the PU data lack labeled-negative instances for training. Recently, there are more and more PU data occurring in practice, such as deceptive review detection [1], text categorization [2] and remote sensing classification [3, 4].

The main difficulty in PU learning is the lack of labeled-negative instances. A natural way to deal with this issue is to pick the instances highly likely to be negative from the unlabeled set and treat them as negative; then the obtained dataset will contain labeled-positive, labeled-negative and unlabeled instances; and thus finally PU learning can be converted to classical semi-supervised learning. The methods following this idea are often referred to as two-step methods [5–12], which can also be generalized to have more steps of further iterative training [13–17].

However, the accuracy of such a multi-step method relies heavily on the accuracy of the algorithm applied in the first step to pick reliable negative instances [18]. This drawback motivated studies to train a PU classifier in a single step, termed one-step methods, which can be further categorized into inconsistent PU learning methods and consistent PU learning methods, depending on if the objective function is a consistent estimator of an expected loss to classify an unknown instance from the population.

A pioneer consistent PU learning method is the unbiased PU learning (uPU) [19]. Subsequently, the non-negative PU learning (nnPU) [20] was proposed by taking the absolute value of the estimated average loss on the negative set in the objective function of uPU for better convergence of the classifier training. Furthermore, imbalanced nnPU (imbalancednnPU) [21] was proposed to address imbalanced PU training set. Nevertheless, the training of the consistent methods often required more information out of the PU dataset, e.g., the class prior or the distribution of population.

Early attempt of the inconsistent PU learning methods was the biased support vector machine (BSVM) [22] based on the classic supervised support vector machine (SVM) [23], assigning a high weight to the average loss of the labeled-positive instances and a low weight to the average loss of the unlabeled instances in the objective function. Subsequently, weighted unlabeled samples SVM (WUS-SVM) [24] was proposed to assign a distinct weight to each of the unlabeled instances according to the likelihood of this unlabeled instance to be negative. Then, the biased least squares SVM (BLS-SVM) was proposed in [25]. It replaces the hinge loss with the squared loss in the objective of BSVM in case that too much importance is given to the unlabeled-positive instances treated as negative during the training of classifier. Then the local constraint was introduced to the objective function of BLS-SVM in [26], encouraging the instances to be classified into the same class as its neighborhoods and the proposed method is called the global and local learning classifier (GLLC). Moreover, the large-margin label-calibrated SVM (LLSVM) [27] was proposed to further alleviate the bias by introducing the hat loss to the objective function, where the hat loss measures the gap between the inverse tangent of the predictive score function (without intercept) and a certain threshold.

However, for trifurcate data where the positive set is roughly constituted by two subsets distributing on both sides of negative instances, existing PU learning methods are usually hard to achieve satisfactory performance. An example of the trifurcate PU datasets is illustrated in Fig. 1 by the 2-dimensional projection with the t-distributed stochastic neighbor embedding (t-SNE) [28] of dataset Wireless Indoor Localization (**wifi**) [29].

A classifier with non-linear decision boundary is needed for the classification of trifurcate datasets. However, when we apply kernel trick to obtain the non-linear

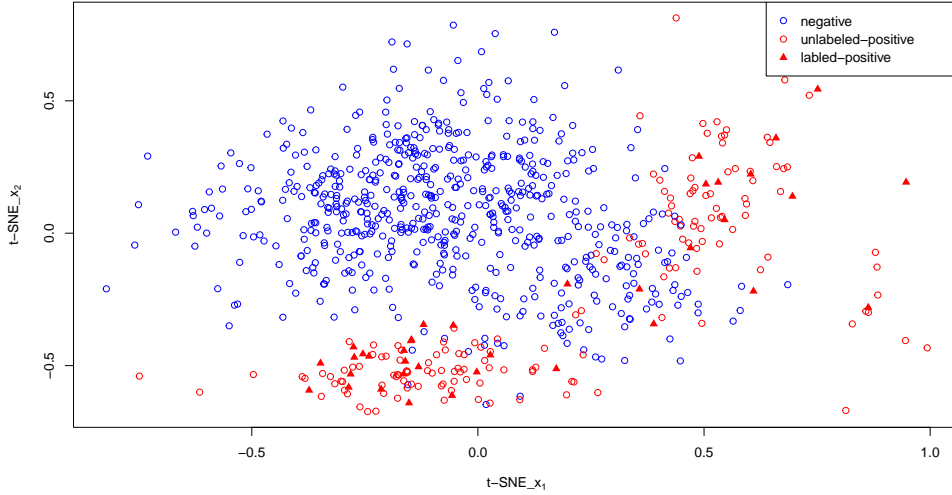


Fig. 1: The 2-dimensional projection with t-SNE of dataset **wifi**, where the positive set is roughly constituted by two subsets distributing on both sides of negative instances; the perplexity for the training of t-SNE on **wifi** was set to 750.

decision boundary, the original trifurcate datasets may be converted to follow the pattern illustrated in Fig. 2, where the distances from the two positive subsets to the ideal decision boundary, as indicated by a solid blue line, are very different. In this case, using the squared loss (e.g. that used in GLLC) will impose quadratic penalty not only on the instances wrongly classified but also on all the instances correctly classified. Therefore, the labeled-positive instances correctly classified by, but far away from, the ideal decision boundary, as circled by the dashed lines in Fig. 2, can unfortunately generate large penalty via the squared loss and hence drag the ideal decision boundary towards the labeled-positive instances far away. This leads to the estimated decision boundary indicated in green solid line, which misclassifies many more instances than the ideal decision boundary.

The aim of applying the squared loss in the objective function of GLLC was to ensure the importance given to the unlabeled-positive instances to be negative support vectors to be lower than the importance given to unlabeled-negative instances to be negative support vectors. Hence we note that it is not necessary to also use the squared loss on the labeled-positive set. Furthermore, we note that, as the hinge loss does not penalise the instances lying on the correct side of the margin, if the hinge loss is applied to the labeled-positive set, the instances correctly classified but far away from the ideal decision boundary will not generate any wrong penalty.

Therefore, motivated by the above analysis, we proposed a PU classifier with asymmetric loss (PUAL) on positive instances for better classification on the trifurcate PU datasets. The contribution of this paper can be summarized as follows.

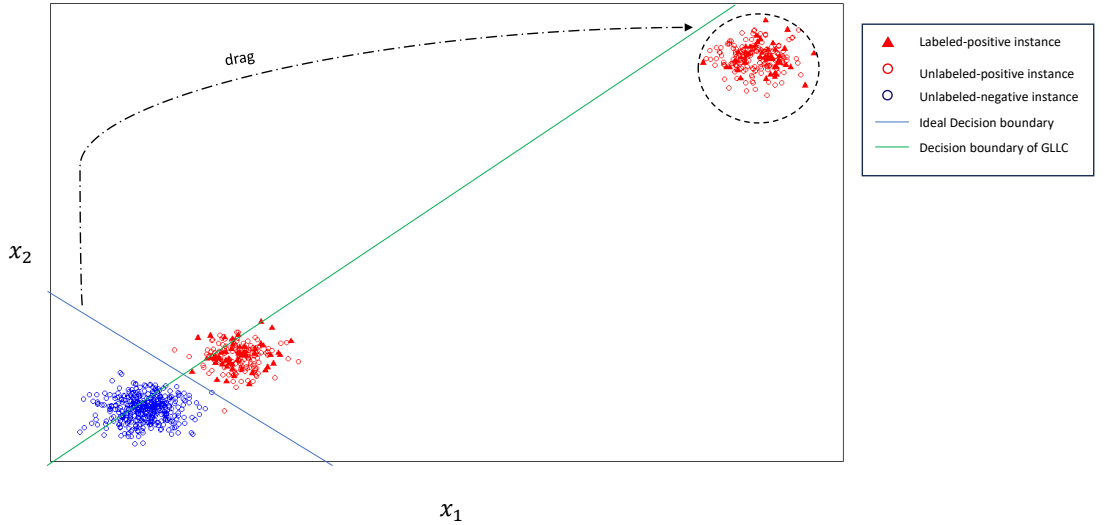


Fig. 2: A pattern of the linearly separable space constructed from the original trifurcate PU datasets via the kernel trick; x_1 and x_2 represent the mappings of the features.

Firstly, in Section 3.1, we propose the methodology and algorithm of PUAL, which can generate a linear decision boundary much closer to the ideal decision boundary for the datasets following the pattern in Fig. 2 but first in the original feature space. This is achieved by using the hinge loss for the labeled-positive instances and the squared loss for the unlabeled-instances (and thus the unlabeled-positive instances).

Secondly, we develop a kernel-based algorithm to enable PUAL to obtain non-linear decision boundary in the original feature space, as detailed in Section 3.2.

Thirdly, we conduct experiments on both simulated and real-world datasets to clearly verify the motivation and effectiveness of our proposed methods, as presented in Section 4.

2 Related Work

Firstly we provide some general definitions involved in the following related works. Suppose there are n_p labeled-positive instances and n_u unlabeled instances with m features. Let feature matrix $\mathbf{X}_{[pu]} = (\mathbf{x}_1, \dots, \mathbf{x}_{n_p}, \dots, \mathbf{x}_{n_p+n_u})^T \in \mathbb{R}^{(n_p+n_u) \times m}$, where the column vector $\mathbf{x}_i \in \mathbb{R}^{m \times 1}$ denotes the vector of the features of the i th instance. Similarly, matrix $\mathbf{X}_{[p]} = (\mathbf{x}_1, \dots, \mathbf{x}_{n_p})^T \in \mathbb{R}^{n_p \times m}$ denotes the feature matrix of the labeled-positive set while matrix $\mathbf{X}_{[u]} = (\mathbf{x}_{n_p+1}, \dots, \mathbf{x}_{n_p+n_u})^T \in \mathbb{R}^{n_u \times m}$ denotes the feature matrix of the unlabeled set. The methods listed in this section are all aimed to train the following predictive score function for classification:

$$f = \mathbf{x}^T \boldsymbol{\beta} + \beta_0, \quad (1)$$

where $\boldsymbol{\beta} = (\beta_1, \beta_2, \dots, \beta_m)^T \in \mathbb{R}^{m \times 1}$ and β_0 are the model parameters.

2.1 BSVM

In order to enable SVM to handle PU classification, BSVM [22] treats all the unlabeled instances as negative and assigns the loss of labeled-positive instances and the loss of unlabeled instances with different weights in the objective function. BSVM trains classifiers by solving the following objective function:

$$\begin{aligned} \min_{\boldsymbol{\beta}, \beta_0} \frac{\lambda}{2} \boldsymbol{\beta}^T \boldsymbol{\beta} + C_p \mathbf{1}_p^T [\mathbf{1}_p - (\mathbf{X}_{[p]} \boldsymbol{\beta} + \mathbf{1}_p \beta_0)]_+ \\ + C_u \mathbf{1}_u^T [\mathbf{1}_u + (\mathbf{X}_{[u]} \boldsymbol{\beta} + \mathbf{1}_u \beta_0)]_+, \end{aligned} \quad (2)$$

where C_p , C_u , and λ are positive hyper-parameters, $[g(\cdot)]_+$ indicates the column vector of the maximum between each element of $g(\cdot)$ and 0, and $\mathbf{1}_{p,u} = \underbrace{(1, 1, \dots, 1)^T}_k$, $k = n_p, n_u$.

2.2 BLS-SVM

One weakness of BSVM is that sometimes the hinge loss in the objective function of BSVM in Equation (2) selects more unlabeled-positive instances than unlabeled-negative instances to be the support vectors for the negative class, which constructs a decision boundary tending to misclassify the unlabeled-positive instances as negative. This is more likely to happen when there are many unlabeled-positive instances close to the unlabeled negative instances.

To deal with this issue, BLS-SVM was proposed by [25] to force all training instances to contribute to the construction of the decision boundary of the trained SVM by solving the following optimization problem:

$$\begin{aligned} \min_{\boldsymbol{\beta}, \beta_0} \frac{\lambda}{2} \boldsymbol{\beta}^T \boldsymbol{\beta} + C_p [\mathbf{1}_p - (\mathbf{X}_{[p]} \boldsymbol{\beta} + \mathbf{1}_p \beta_0)]^T [\mathbf{1}_p - (\mathbf{X}_{[p]} \boldsymbol{\beta} + \mathbf{1}_p \beta_0)] \\ + C_u [\mathbf{1}_u + (\mathbf{X}_{[u]} \boldsymbol{\beta} + \mathbf{1}_u \beta_0)]^T [\mathbf{1}_u + (\mathbf{X}_{[u]} \boldsymbol{\beta} + \mathbf{1}_u \beta_0)], \end{aligned} \quad (3)$$

where the squared loss replaces the hinge loss in BSVM on both labeled-positive set and unlabeled set. The objective function of BLS-SVM makes all the instances contribute to the construction of the decision boundary hence the importance given to the unlabeled-positive instances treated as negative is restricted [30].

2.3 GLLC

The similarities between a training instance and its neighbors can also be treated as a factor for classification, the idea of which is named local learning [31]. It is noted that the gap between PU learning and classical supervised learning on accuracy can be mitigated via GLLC [26], which is a combination of BLS-SVM and local learning.

The objective function of GLLC is given as

$$\begin{aligned} \min_{\boldsymbol{\beta}, \beta_0} & \frac{\lambda}{2} \boldsymbol{\beta}^T \boldsymbol{\beta} + C_p [\mathbf{1}_p - (\mathbf{X}_{[p]} \boldsymbol{\beta} + \mathbf{1}_p \beta_0)]^T [\mathbf{1}_p - (\mathbf{X}_{[p]} \boldsymbol{\beta} + \mathbf{1}_p \beta_0)] \\ & + C_u [\mathbf{1}_u + (\mathbf{X}_{[u]} \boldsymbol{\beta} + \mathbf{1}_u \beta_0)]^T [\mathbf{1}_u + (\mathbf{X}_{[u]} \boldsymbol{\beta} + \mathbf{1}_u \beta_0)] \\ & + (\mathbf{X}_{[pu]} \boldsymbol{\beta} + \mathbf{1}_{pu} \beta_0)^T \mathbf{R} (\mathbf{X}_{[pu]} \boldsymbol{\beta} + \mathbf{1}_{pu} \beta_0), \end{aligned} \quad (4)$$

where \mathbf{R} is the similarity matrix for the instances and their neighbors, which can be calculated as follows.

Firstly we need to calculate matrix \mathbf{W} by

$$w_{ij} = \begin{cases} \exp(-\sigma^{-1}(\mathbf{x}_i - \mathbf{x}_j)^T(\mathbf{x}_i - \mathbf{x}_j)) & \text{if the } i\text{th and } j\text{th instances are KNN of each other,} \\ 0 & \text{otherwise,} \end{cases} \quad (5)$$

where σ is a hyper-parameter to be selected. Then defining $\mathbf{1}_{pu} = \underbrace{(1, 1, \dots, 1)}_k$, $k = n_p + n_u$ and letting \mathbf{w}_i denote the i th column of matrix \mathbf{W} and \mathbf{W}^* denote a diagonal matrix with the i th diagonal element equal to $\mathbf{1}_{[pu]}^T \mathbf{w}_i$, one can obtain

$$\mathbf{R} = \frac{1}{(n_p + n_u)} (\mathbf{W}^* - \mathbf{W}). \quad (6)$$

3 Methodology

3.1 PUAL with Linear Decision Boundary

3.1.1 Objective Function

As discussed in Section 1, we propose to apply the hinge loss to the labeled-positive instances, so as to impose no penalty to the instances correctly classified but far away from the ideal decision boundary. Meanwhile, the squared loss needs to be applied to the unlabeled instances in case that too much importance is given to the unlabeled-positive instances treated as negative during the training of the classifier. Hence we propose a structure of asymmetric loss on positive instances to revise GLLC, so that the new method PUAL is able to address the issue of classification of trifurcate PU data. Moreover, a local constraint term of similarity is helpful for PU classification. Therefore, the unconstrained optimization problem of PUAL can be formulated as

$$\begin{aligned} \min_{\boldsymbol{\beta}, \beta_0} & \frac{\lambda}{2} \boldsymbol{\beta}^T \boldsymbol{\beta} + C_p \mathbf{1}_p^T [\mathbf{1}_p - (\mathbf{X}_{[p]} \boldsymbol{\beta} + \mathbf{1}_p \beta_0)]_+ \\ & + C_u [\mathbf{1}_u + (\mathbf{X}_{[u]} \boldsymbol{\beta} + \mathbf{1}_u \beta_0)]^T [\mathbf{1}_u + (\mathbf{X}_{[u]} \boldsymbol{\beta} + \mathbf{1}_u \beta_0)] \\ & + (\mathbf{X}_{[pu]} \boldsymbol{\beta} + \mathbf{1}_{pu} \beta_0)^T \mathbf{R} (\mathbf{X}_{[pu]} \boldsymbol{\beta} + \mathbf{1}_{pu} \beta_0). \end{aligned} \quad (7)$$

However, the hinge loss term $\mathbf{1}_p^T [\mathbf{1}_p - (\mathbf{X}_{[p]} \boldsymbol{\beta} + \mathbf{1}_p \beta_0)]_+$ in the objective function of PUAL in Equation (7) is not always differentiable in the feasible region of the

optimization, bringing difficulty to applying the gradient descent directly. To find an alternative way for solving PUAL, the following reformulation of Equation (7) can be considered:

$$\begin{aligned}
& \min_{\boldsymbol{\beta}, \beta_0, \mathbf{h}} C_p \mathbf{1}_p^T [\mathbf{h}]_+ + C_u (\mathbf{1}_u + \mathbf{X}_{[u]} \boldsymbol{\beta} + \mathbf{1}_u \beta_0)^T (\mathbf{1}_u + \mathbf{X}_{[u]} \boldsymbol{\beta} + \mathbf{1}_u \beta_0) \\
& + (\mathbf{X}_{[pu]} \boldsymbol{\beta} + \mathbf{1}_{pu} \beta_0)^T \mathbf{R} (\mathbf{X}_{[pu]} \boldsymbol{\beta} + \mathbf{1}_{pu} \beta_0) + \frac{\lambda}{2} \boldsymbol{\beta}^T \boldsymbol{\beta} \\
& \text{s.t. } \mathbf{h} = \mathbf{1}_p - (\mathbf{X}_{[p]} \boldsymbol{\beta} + \mathbf{1}_p \beta_0).
\end{aligned} \tag{8}$$

The predictive score function of PUAL for instance \mathbf{x} is the same as the predictive score function of SVM in Equation (1).

3.1.2 Parameter Estimation

The convex objective function in Equation (8) can be regarded as the sum of the functions of $(\boldsymbol{\beta}, \beta_0)$ and the function of \mathbf{h} while the constraints in Equation (8) can be regarded as a linear combination of $(\boldsymbol{\beta}, \beta_0)$ and \mathbf{h} ; this meets the requirement of ADMM [32, 33], which can decompose a large-scale convex optimization problem with affine constraints into several simpler sub-problems and update the solution iteratively until convergence. Moreover, ADMM is able to converge to modest accuracy within fewer iterations than the gradient descent. Hence, we adopt it here.

The Lagrangian function of problem in Equation (8) is

$$\begin{aligned}
\mathcal{L}(\boldsymbol{\theta}) = & C_p \mathbf{1}_p^T [\mathbf{h}]_+ + C_u (\mathbf{1}_u + \mathbf{X}_{[u]} \boldsymbol{\beta} + \mathbf{1}_u \beta_0)^T (\mathbf{1}_u + \mathbf{X}_{[u]} \boldsymbol{\beta} + \mathbf{1}_u \beta_0) \\
& + (\mathbf{X}_{[pu]} \boldsymbol{\beta} + \mathbf{1}_{pu} \beta_0)^T \mathbf{R} (\mathbf{X}_{[pu]} \boldsymbol{\beta} + \mathbf{1}_{pu} \beta_0) + \frac{\lambda}{2} \boldsymbol{\beta}^T \boldsymbol{\beta} \\
& + \mathbf{u}_h^T [\mathbf{1}_p - (\mathbf{X}_{[p]} \boldsymbol{\beta} + \mathbf{1}_p \beta_0) - \mathbf{h}],
\end{aligned} \tag{9}$$

where $\boldsymbol{\theta} = \{\boldsymbol{\beta}, \beta_0, \mathbf{h}, \mathbf{u}_h\}$ and \mathbf{u}_h is dual variable. Then the augmented Lagrangian function is given as

$$\mathcal{L}_a(\boldsymbol{\theta}) = \mathcal{L}(\boldsymbol{\theta}) + \frac{\mu_1}{2} \left\| \mathbf{1}_p - (\mathbf{X}_{[p]} \boldsymbol{\beta} + \mathbf{1}_p \beta_0) - \mathbf{h} \right\|_2^2, \tag{10}$$

where μ_1 is the step-size coefficient of the augmented Lagrangian function.

It follows that the update of $\boldsymbol{\beta}$ and β_0 is

$$\begin{aligned}
(\boldsymbol{\beta}^{(k+1)}, \beta_0^{(k+1)}) = & \arg \min_{\boldsymbol{\beta}, \beta_0} \frac{\lambda}{2} \boldsymbol{\beta}^T \boldsymbol{\beta} \\
& + C_u (\mathbf{1}_u + \mathbf{X}_{[u]} \boldsymbol{\beta} + \mathbf{1}_u \beta_0)^T (\mathbf{1}_u + \mathbf{X}_{[u]} \boldsymbol{\beta} + \mathbf{1}_u \beta_0) \\
& + (\mathbf{X}_{[pu]} \boldsymbol{\beta} + \mathbf{1}_{pu} \beta_0)^T \mathbf{R} (\mathbf{X}_{[pu]} \boldsymbol{\beta} + \mathbf{1}_{pu} \beta_0) \\
& + \mathbf{u}_h^{(k)T} [\mathbf{1}_p - (\mathbf{X}_{[p]} \boldsymbol{\beta} + \mathbf{1}_p \beta_0) - \mathbf{h}^{(k)}] \\
& + \frac{\mu_1}{2} \left\| \mathbf{1}_p - (\mathbf{X}_{[p]} \boldsymbol{\beta} + \mathbf{1}_p \beta_0) - \mathbf{h}^{(k)} \right\|_2^2,
\end{aligned} \tag{11}$$

which is a quadratic optimization with every term differentiable. Let $\mathbf{I}_k, \forall k \in \mathbb{Z}$, denote a $k \times k$ identity matrix. By defining

$$\begin{aligned}
\mathbf{M}_{11} &= \lambda \mathbf{I}_m + 2C_u \mathbf{X}_{[u]}^T \mathbf{X}_{[u]} + 2\mathbf{X}_{[pu]}^T \mathbf{R} \mathbf{X}_{[pu]} + \mu_1 \mathbf{X}_{[p]}^T \mathbf{X}_{[p]}, \\
\mathbf{M}_{12} &= 2C_u \mathbf{X}_{[u]}^T \mathbf{1}_u + 2\mathbf{X}_{[pu]}^T \mathbf{R} \mathbf{1}_{pu} + \mu_1 \mathbf{X}_{[p]}^T \mathbf{1}_p, \\
\mathbf{M}_{21} &= 2C_u \mathbf{1}_u^T \mathbf{X}_{[u]} + 2\mathbf{1}_{pu}^T \mathbf{R} \mathbf{X}_{[pu]} + \mu_1 \mathbf{1}_p^T \mathbf{X}_{[p]}, \\
\mathbf{M}_{22} &= 2C_u n_u + 2\mathbf{1}_{pu}^T \mathbf{R} \mathbf{1}_{pu} + \mu_1 n_p, \\
\mathbf{m}_1 &= -2C_u \mathbf{X}_{[u]}^T \mathbf{1}_u + \mathbf{X}_{[p]}^T \mathbf{u}_h + \mu_1 \mathbf{X}_{[p]}^T (\mathbf{1}_p - \mathbf{h}), \\
\mathbf{m}_2 &= -2C_u n_u + \mathbf{u}_h^T \mathbf{1}_p + \mu_1 (\mathbf{1}_p - \mathbf{h})^T \mathbf{1}_p,
\end{aligned} \tag{12}$$

the solution of problem in Equation (11) can be obtained by solving the following linear equation w.r.t. $\boldsymbol{\beta}$ and β_0 :

$$\begin{bmatrix} \mathbf{M}_{11} & \mathbf{M}_{12} \\ \mathbf{M}_{21} & \mathbf{M}_{22} \end{bmatrix} \begin{bmatrix} \boldsymbol{\beta}^{(k+1)} \\ \beta_0^{(k+1)} \end{bmatrix} = \begin{bmatrix} \mathbf{m}_1 \\ m_2 \end{bmatrix}. \tag{13}$$

Then the update of \mathbf{h} becomes

$$\begin{aligned}
\mathbf{h}^{(k+1)} &= \arg \min_{\mathbf{h}} C_p \mathbf{1}_p^T [\mathbf{h}]_+ + \mathbf{u}_h^{(k)T} [\mathbf{1}_p - (\mathbf{X}_{[p]} \boldsymbol{\beta}^{(k+1)} + \mathbf{1}_p \beta_0^{(k+1)}) - \mathbf{h}] \\
&\quad + \frac{\mu_1}{2} \left\| \mathbf{1}_p - (\mathbf{X}_{[p]} \boldsymbol{\beta}^{(k+1)} + \mathbf{1}_p \beta_0^{(k+1)}) - \mathbf{h} \right\|_2^2,
\end{aligned} \tag{14}$$

which is equivalent to solving the problem

$$\min_{\mathbf{h}} \sum_{i=1}^{n_p} \left\{ \frac{C_p}{\mu_1} [h_i]_+ + \frac{1}{2} \left[1 + \frac{u_{hi}^{(k)}}{\mu_1} - (\mathbf{x}_i^T \boldsymbol{\beta}^{(k+1)} + \beta_0^{(k+1)}) - h_i \right]^2 \right\}. \tag{15}$$

According to [34], for constant $c > 0$, we can obtain

$$\arg \min_x c[x]_+ + \frac{1}{2} \|x - d\|_2^2 = \begin{cases} d - c & d > c, \\ 0 & 0 \leq d \leq c, \\ d & d < 0. \end{cases} \tag{16}$$

Thus, by defining $s_c(d) = \arg \min_x c[x]_+ + \frac{1}{2} \|x - d\|_2^2$, the i th element of $\mathbf{h}^{(k+1)}$ in problem in Equation (14) is solved as

$$h_i^{(k+1)} = s_{\frac{C_p}{\mu_1}} \left(1 + \frac{u_{hi}^{(k)}}{\mu_1} - (\mathbf{x}_i^T \boldsymbol{\beta}^{(k+1)} + \beta_0^{(k+1)}) \right), i = 1, \dots, n_p. \tag{17}$$

According to [33], the update of the dual parameter \mathbf{u}_h can be

$$\mathbf{u}_h^{(k+1)} = \mathbf{u}_h^{(k)} + \mu_1[\mathbf{1}_p - (\mathbf{X}_{[p]}\boldsymbol{\beta}^{(k+1)} + \mathbf{1}_p\beta_0^{(k+1)}) - \mathbf{h}^{(k+1)}]. \quad (18)$$

3.1.3 Algorithm

The algorithm of PUAL can be summarized in Algorithm 1.

Algorithm 1 PUAL with linear decision boundary

Input: PU dataset, C_p , C_u , λ , σ and μ_1

Output: $\boldsymbol{\beta}$ and β_0

- 1: Initialize $\boldsymbol{\beta}$, β_0 , \mathbf{h} , \mathbf{u}_h
 - 2: **while** not converged **do**
 - 3: Update $(\boldsymbol{\beta}^{(k+1)}, \beta_0^{(k+1)}) = \arg \min_{\boldsymbol{\beta}, \beta_0} \mathcal{L}_a(\boldsymbol{\beta}, \beta_0, \mathbf{h}^{(k)}, \mathbf{u}_h^{(k)})$
 - 4: Update $\mathbf{h}^{(k+1)} = \arg \min_{\mathbf{h}} \mathcal{L}_a(\boldsymbol{\beta}^{(k+1)}, \beta_0^{(k+1)}, \mathbf{h}, \mathbf{u}_h^{(k)})$
 - 5: Update $\mathbf{u}_h^{(k+1)} = \mathbf{u}_h^{(k)} + \mu_1[\mathbf{1}_p - (\mathbf{X}_{[p]}\boldsymbol{\beta}^{(k+1)} + \mathbf{1}_p\beta_0^{(k+1)}) - \mathbf{h}^{(k+1)}]$
 - 6: **end while**
-

3.2 PUAL with Non-Linear Decision Boundary

In this section, we develop a kernel-based algorithm to enable PUAL to have non-linear decision boundary, so that PUAL can be applied on the non-linear separable datasets including trifurcate PU datasets. The techniques applied in this section are similar to many previous methods [26, 35–37].

3.2.1 Objective Function

Suppose $\phi(\mathbf{x}) \in \mathbb{R}^{r \times 1}$ be a mapping of the instance vector \mathbf{x} . Then let $\phi(\mathbf{X}_{[k]}) \in \mathbb{R}^{n_k \times r}$, $k = p, u, pu$ be the mapping of the original data matrix $\mathbf{X}_{[k]}$. The i th row of $\phi(\mathbf{X}_{[k]})$ is $\phi(\mathbf{x}_i)^T$. According to Equations (12) and (13), using $\phi(\mathbf{X}_{[k]})$ as features matrix instead of $\mathbf{X}_{[k]}$ for the training of PUAL, we can find the following necessary condition for the optimal solution of $\boldsymbol{\beta}$:

$$\mathbf{B}\boldsymbol{\beta} = \phi(\mathbf{X}_{[pu]})^T \boldsymbol{\Omega}, \quad (19)$$

where

$$\mathbf{B} = \mathbf{M}_{11} - \frac{\mathbf{M}_{12}\mathbf{M}_{21}}{\mathbf{M}_{22}}, \quad (20)$$

and

$$\boldsymbol{\Omega} = \begin{bmatrix} \mathbf{u}_h - \mu_1 \frac{m_2}{M_{22}} \mathbf{1}_p + \mu_1 (\mathbf{1}_p - \mathbf{h}) \\ -2C_u \mathbf{1}_u - 2 \frac{m_2}{M_{22}} C_u \mathbf{1}_u \end{bmatrix} - 2 \frac{m_2}{M_{22}} \mathbf{R} \mathbf{1}_{pu}. \quad (21)$$

Equation (19) can be regarded as a condition when the objective function reaches its minimum. For $n_p, n_u > m$, \mathbf{B} is symmetric and invertible. In this case, we can obtain

$$\boldsymbol{\beta} = \mathbf{B}^{-1} \boldsymbol{\phi}(\mathbf{X}_{[pu]})^T \boldsymbol{\Omega}. \quad (22)$$

Substituting Equation (22) into the objective function in Equation (7), we have the new objective function as

$$\begin{aligned} \min_{\boldsymbol{\Omega}, \beta_0} \frac{\lambda}{2} \boldsymbol{\Omega}^T \boldsymbol{\phi}(\mathbf{X}_{[pu]}) \mathbf{B}^{-1} \mathbf{B}^{-1} \boldsymbol{\phi}(\mathbf{X}_{[pu]})^T \boldsymbol{\Omega} + C_p \mathbf{1}_p^T [\mathbf{1}_p - (\boldsymbol{\phi}(\mathbf{X}_{[p]}) \mathbf{B}^{-1} \boldsymbol{\phi}(\mathbf{X}_{[pu]})^T \boldsymbol{\Omega} + \mathbf{1}_p \beta_0)]_+ \\ + C_u [\mathbf{1}_u + \boldsymbol{\phi}(\mathbf{X}_{[u]}) \mathbf{B}^{-1} \boldsymbol{\phi}(\mathbf{X}_{[pu]})^T \boldsymbol{\Omega} + \mathbf{1}_u \beta_0] [\mathbf{1}_u + \boldsymbol{\phi}(\mathbf{X}_{[u]}) \mathbf{B}^{-1} \boldsymbol{\phi}(\mathbf{X}_{[pu]})^T \boldsymbol{\Omega} + \mathbf{1}_u \beta_0]^T \\ + (\boldsymbol{\phi}(\mathbf{X}_{[pu]}) \mathbf{B}^{-1} \boldsymbol{\phi}(\mathbf{X}_{[pu]})^T \boldsymbol{\Omega} + \mathbf{1}_{pu} \beta_0)^T \mathbf{R} (\boldsymbol{\phi}(\mathbf{X}_{[pu]}) \mathbf{B}^{-1} \boldsymbol{\phi}(\mathbf{X}_{[pu]})^T \boldsymbol{\Omega} + \mathbf{1}_{pu} \beta_0). \end{aligned} \quad (23)$$

To prove $\boldsymbol{\phi}(\mathbf{X}_{[k]}) \mathbf{B}^{-1} \boldsymbol{\phi}(\mathbf{X}_{[pu]})^T$ and $\boldsymbol{\phi}(\mathbf{X}_{[k]}) \mathbf{B}^{-1} \mathbf{B}^{-1} \boldsymbol{\phi}(\mathbf{X}_{[pu]})^T$ in Equation (23) are kernel matrices for $\mathbf{X}_{[k]}$ and $\mathbf{X}_{[pu]}$, we need to introduce the two closure properties for the construction of kernel functions proved in [38] as follows.

Theorem 1. Let $\boldsymbol{\phi}(\mathbf{X}), \boldsymbol{\phi}(\mathbf{Z})$ be a mapping of matrices of \mathbf{X}, \mathbf{Z} and $\boldsymbol{\kappa}_1(\boldsymbol{\phi}(\mathbf{X}), \boldsymbol{\phi}(\mathbf{Z}))$ be a kernel matrix of $\boldsymbol{\phi}(\mathbf{X})$ and $\boldsymbol{\phi}(\mathbf{Z})$. Then the following two matrices $\boldsymbol{\kappa}_2(\mathbf{X}, \mathbf{Z})$ and $\boldsymbol{\kappa}_3(\mathbf{X}, \mathbf{Z})$ can be regarded as the kernel matrix w.r.t. \mathbf{X}, \mathbf{Z} :

- $\boldsymbol{\kappa}_2(\mathbf{X}, \mathbf{Z}) = \boldsymbol{\kappa}_1(\boldsymbol{\phi}(\mathbf{X}), \boldsymbol{\phi}(\mathbf{Z}))$,
- $\boldsymbol{\kappa}_3(\mathbf{X}, \mathbf{Z}) = \mathbf{X} \mathbf{F} \mathbf{Z}^T$, with \mathbf{F} to be a symmetric matrix.

Then, according to the closure properties in Theorem 1, we can obtain

$$\begin{aligned} \boldsymbol{\phi}(\mathbf{X}_{[k]}) \mathbf{B}^{-1} \boldsymbol{\phi}(\mathbf{X}_{[pu]})^T &= \boldsymbol{\Phi}'(\boldsymbol{\phi}(\mathbf{X}_{[k]}), \boldsymbol{\phi}(\mathbf{X}_{[pu]})) \\ &= \boldsymbol{\Phi}(\mathbf{X}_{[k]}, \mathbf{X}_{[pu]}) \end{aligned} \quad (24)$$

and

$$\begin{aligned} \boldsymbol{\phi}(\mathbf{X}_{[k]}) \mathbf{B}^{-1} \mathbf{B}^{-1} \boldsymbol{\phi}(\mathbf{X}_{[pu]})^T &= \boldsymbol{\Phi}''(\boldsymbol{\phi}(\mathbf{X}_{[k]}), \boldsymbol{\phi}(\mathbf{X}_{[pu]})) \\ &= \boldsymbol{\Phi}_2(\mathbf{X}_{[k]}, \mathbf{X}_{[pu]}), \end{aligned} \quad (25)$$

where $\boldsymbol{\Phi}'(\boldsymbol{\phi}(\mathbf{X}_{[k]}), \boldsymbol{\phi}(\mathbf{X}_{[pu]}))$, $\boldsymbol{\Phi}''(\boldsymbol{\phi}(\mathbf{X}_{[k]}), \boldsymbol{\phi}(\mathbf{X}_{[pu]}))$ are the kernel matrices for $\boldsymbol{\phi}(\mathbf{X}_{[k]})$ and $\boldsymbol{\phi}(\mathbf{X}_{[pu]})$, and $\boldsymbol{\Phi}(\mathbf{X}_{[k]}, \mathbf{X}_{[pu]})$, $\boldsymbol{\Phi}_2(\mathbf{X}_{[k]}, \mathbf{X}_{[pu]})$ are the kernel matrices for $\mathbf{X}_{[k]}$ and $\mathbf{X}_{[pu]}$.

Hence, the objective function of PUAL can be reformulated as

$$\begin{aligned} \min_{\boldsymbol{\Omega}, \beta_0} \frac{\lambda}{2} \boldsymbol{\Omega}^T \boldsymbol{\Phi}_2(\mathbf{X}_{[pu]}, \mathbf{X}_{[pu]}) \boldsymbol{\Omega} + C_p \mathbf{1}_p^T [\mathbf{1}_p - (\boldsymbol{\Phi}(\mathbf{X}_{[p]}, \mathbf{X}_{[pu]}) \boldsymbol{\Omega} + \mathbf{1}_p \beta_0)]_+ \\ + C_u [\mathbf{1}_u + \boldsymbol{\Phi}(\mathbf{X}_{[u]}, \mathbf{X}_{[pu]}) \boldsymbol{\Omega} + \mathbf{1}_u \beta_0]^T [\mathbf{1}_u + \boldsymbol{\Phi}(\mathbf{X}_{[u]}, \mathbf{X}_{[pu]}) \boldsymbol{\Omega} + \mathbf{1}_u \beta_0] \\ + (\boldsymbol{\Phi}(\mathbf{X}_{[pu]}, \mathbf{X}_{[pu]}) \boldsymbol{\Omega} + \mathbf{1}_{pu} \beta_0)^T \mathbf{R} (\boldsymbol{\Phi}(\mathbf{X}_{[pu]}, \mathbf{X}_{[pu]}) \boldsymbol{\Omega} + \mathbf{1}_{pu} \beta_0), \end{aligned} \quad (26)$$

whose solution is not related to $\mathbf{X}_{[k]}$, $k = p.u.pu$ once the kernel matrices are determined.

The predictive score function for instance \mathbf{x}^* of PUAL can be now transformed to

$$f = \boldsymbol{\Phi}(\mathbf{x}^*, \mathbf{X}_{[pu]}) \boldsymbol{\Omega} + \beta_0. \quad (27)$$

3.2.2 Parameter Estimation

In this case, we can update β_0 via

$$\beta_0^{(k+1)} = \frac{m_2}{M_{22}} - \mathbf{Q}_b^{(k+1)} / M_{22}, \quad (28)$$

where m_2 , M_{22} are not related to $\mathbf{X}_{[p]}$, $\mathbf{X}_{[u]}$, $\mathbf{X}_{[pu]}$ and

$$\begin{aligned} \mathbf{Q}_b^{(k+1)} = & 2C_u \mathbf{1}_u^T \Phi(\mathbf{X}_{[u]}, \mathbf{X}_{[pu]}) \Omega^{(k+1)} \\ & + 2\mathbf{1}_{pu}^T \mathbf{R} \Phi(\mathbf{X}_{[pu]}, \mathbf{X}_{[pu]}) \Omega^{(k+1)} \\ & + \mu_1 \mathbf{1}_p^T \Phi(\mathbf{X}_{[p]}, \mathbf{X}_{[pu]}) \Omega^{(k+1)}. \end{aligned} \quad (29)$$

The update of \mathbf{h} , \mathbf{u}_h can be reformulated as

$$\begin{aligned} \mathbf{h}_i^{(k+1)} = & s_{\frac{C_p}{\mu_1}} \left(1 + \frac{u_{hi}^{(k)}}{\mu_1} - (\Phi(\mathbf{x}_i, \mathbf{X}_{[pu]}) \Omega^{(k+1)} + \beta_0^{(k+1)}) \right), i = 1, \dots, n_p, \\ \mathbf{u}_h^{(k+1)} = & \mathbf{u}_h^{(k)} + \mu_1 [\mathbf{1}_p - (\Phi(\mathbf{X}_{[p]}, \mathbf{X}_{[pu]}) \Omega^{(k+1)} + \mathbf{1}_p \beta_0^{(k+1)}) - \mathbf{h}^{(k+1)}]. \end{aligned} \quad (30)$$

As $\Phi_2(\mathbf{X}_{[k]}, \mathbf{X}_{[pu]})$ does not directly appear in the update process for the optimization, we only need to determine the form of $\Phi(\mathbf{X}_{[k]}, \mathbf{X}_{[pu]})$ in practice. Moreover, λ either does not appear directly in the above update process or it is contained in the matrix \mathbf{B} as a part of $\Phi(\mathbf{X}_{[k]}, \mathbf{X}_{[pu]})$. Therefore, for convenience, in the case of using the kernel trick in Section 4.1, we use λ to represent the hyper-parameter(s) of the kernel matrix $\Phi(\mathbf{X}_{[k]}, \mathbf{X}_{[pu]})$.

3.2.3 Algorithm

The algorithm of PUAL with non-linear decision boundary can be summarized in Algorithm 2.

Algorithm 2 PUAL with non-linear decision boundary

Input: PU dataset, Φ , C_p , C_u , λ , σ and μ_1

Output: Ω and β_0

- 1: Initialize Ω , β_0 , \mathbf{h} , \mathbf{u}_h .
 - 2: **while** not converged **do**
 - 3: Update Ω via Equation (21) w.r.t. $\mathbf{h}^{(k)}$ and $\mathbf{u}_h^{(k)}$
 - 4: Update β_0 via Equation (28)
 - 5: Update \mathbf{h} , \mathbf{u}_h via Equation (30)
 - 6: **end while**
-

4 Experiments

4.1 Experiments on Synthetic Data

In this section, we conduct experiments on synthetic datasets following the pattern in Fig. 2 to verify the superior performance of PUAL over GLLC.

4.1.1 Generation of Synthetic Positive-Negative (PN) Datasets

The synthetic datasets following the pattern in Fig. 2 were obtained by the following steps:

1. To generate the first subset of the 2-dimensional synthetic positive set, 200 instances were sampled from the multivariate normal distribution with mean vector $(15, 15)$ and the covariance matrix $\begin{bmatrix} 50 & 0 \\ 0 & 50 \end{bmatrix}$.
2. To generate the second subset of the 2-dimensional synthetic positive set, 200 instances were sampled from the multivariate normal distribution with the mean vector $(\mathbf{mean}_{p2}, \mathbf{mean}_{p2})$ and the covariance matrix $\begin{bmatrix} 50 & 0 \\ 0 & 50 \end{bmatrix}$.
3. To generate the 2-dimensional synthetic negative set, 400 instances were sampled from the multivariate normal distribution of mean vector $(0, 0)$ and the covariance matrix $\begin{bmatrix} 50 & 0.2 \\ 0.2 & 50 \end{bmatrix}$.
4. Mixing the first subset of the synthetic positive set obtained in Step 1, the second subset of the synthetic positive set obtained in Step 2 and the synthetic negative set obtained in Step 3, a simple 2-dimensional synthetic dataset can be eventually obtained as shown in Fig. 2.

In Step 2, \mathbf{mean}_{p2} took value from $(50, 100, 200, 500, 1000)$. For each value of \mathbf{mean}_{p2} , the above steps were repeated 5 times so that we have 5 synthetic datasets for each value of \mathbf{mean}_{p2} .

4.1.2 Training-Test Split for the Synthetic PU Datasets

It should be noted that both GLLC and PUAL can be applied on the datasets sampled from either single-training-set scenario [39] or case-control scenario [19] as we set the suitable metric for hyper-parameter tuning in practice. More specifically, the case-control scenario indicates that the unlabeled training set can be regarded to be i.i.d. sampled from the population, while the single-training-set scenario indicates that the whole training set can be regarded to be i.i.d. sampled from the population. In this case, for more intuitive comparison, we split each of the synthetic dataset generated in Section 4.1.1 to construct the PU training and test sets consistent with the single-training-set scenario by the following two steps:

1. Firstly, to split the dataset into a training set and a test set, 70% of the instances in the simple synthetic dataset obtained in Section 4.1.1 were randomly selected as the training set while the test set was constituted by the rest 30% instances.

- Secondly, to construct the labeled-positive set and unlabeled-set for training, 25% of the positive instances in the above obtained training set were randomly selected to form the labeled-positive set for training. The rest of the positive instances were mixed with the negative set, contributing to the unlabeled set for training.

Then 25 pairs of PU training set and test set were obtained.

4.1.3 Model Setting

We note that the real value of F1-score on the training dataset is not accessible if we do not use the label information during model training. Therefore, by fixing C_p to 1 and the number K of the nearest neighbors to 5, C_u , λ , σ in the objective functions of PUAL and GLLC were determined by 4-fold cross-validation (CV), which reached the highest average PUF-score proposed in [40] on the validation sets. PUF-score is similar to F1-score and can be directly obtained from PU data:

$$\text{PUF-score} = \frac{\text{recall}^2}{P[\text{sgn}(f(\mathbf{x})) = 1]}, \quad (31)$$

where ‘recall’ can be estimated by computing $\frac{1}{n_p} \sum_{\mathbf{x}_i \in X_{[p]}} \mathbb{1}(\text{sgn}(f(\mathbf{x}_i)) = 1)$ with the indicator function denoted by $\mathbb{1}(\cdot)$, and at the single-training-set scenario $P[\text{sgn}(f(\mathbf{x})) = 1]$ can be estimated by computing $\frac{1}{n_p+n_u} \sum_{\mathbf{x}_i \in X_{[pu]}} \mathbb{1}(\text{sgn}(f(\mathbf{x}_i)) = 1)$. Furthermore, λ , σ were tuned from the set $\{1, 2, 3, 4, 5\} \circ \{0.1, 1, 10, 100\}$; C_u was selected from the set $\{0.01, 0.02, \dots, 0.5\}$ based on the setting in [26].

4.1.4 Results and Analysis

Results of the experiments on the constructed synthetic PU datasets are summarized in Table 1. The performance are measured by the average F1-score, which is a widely-used metric for the evaluation of PU learning methods [41]. The patterns of the decision boundary obtained by PUAL and GLLC on the synthetic datasets are illustrated in Fig. 3. For each value of \mathbf{mean}_{p2} , we use the first generated synthetic dataset as example.

According to the experimental results in Table 1, PUAL always has better performance than GLLC on the synthetic PU datasets with all the 5 values of \mathbf{mean}_{p2} . Furthermore, with the value of \mathbf{mean}_{p2} increasing, the gap between PUAL and GLLC becomes increasingly large. This is more clearly in the six plots in Fig. 3, as one of the positive subset becomes increasingly far away, the decision boundary of GLLC is dragged to a strange position that more and more instances are misclassified by the decision boundary of GLLC, while the decision boundary of PUAL is unaffected. Therefore, it is verified that PUAL can generate much better linear decision boundary than GLLC on the datasets following the pattern in Fig. 2.

4.2 Experiments on Real-World Data

In this section, we further assess the classification performance of PUAL on real-world datasets.

Table 1: Summary of the average F1-score (%) with the standard deviation, from the experiments on the synthetic dataset; the result highlighted in blue is the better one between PUAL and GLLC.

\mathbf{mean}_{p_2}	PUAL	GLLC
50	95.07 \pm 0.78	91.17 \pm 1.52
100	94.89 \pm 0.61	86.27 \pm 1.83
200	93.56 \pm 0.75	81.04 \pm 2.93
500	92.83 \pm 3.22	73.58 \pm 2.58
1000	93.47 \pm 2.08	71.28 \pm 2.37

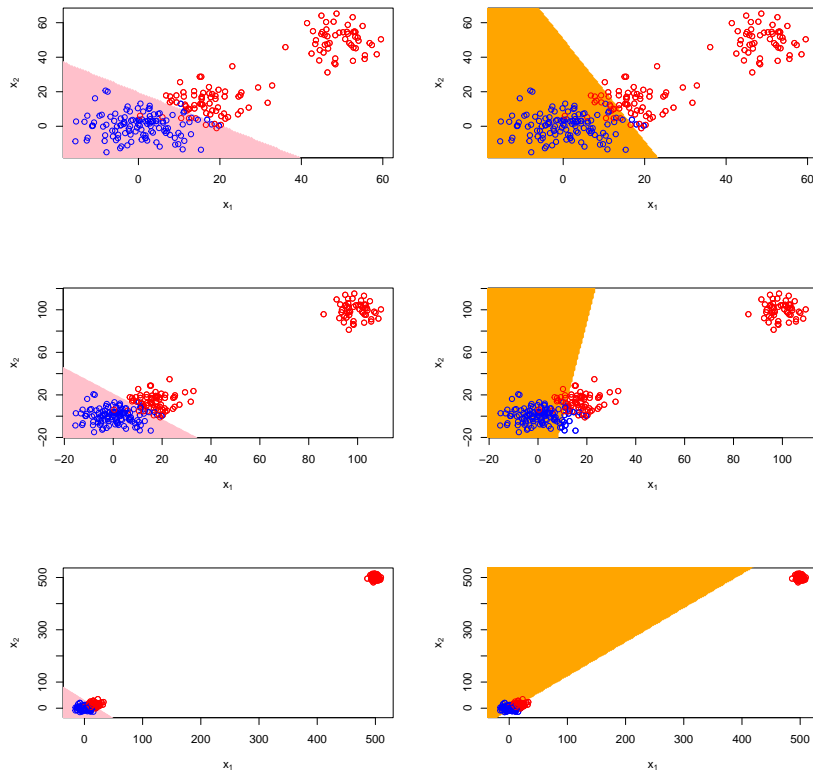


Fig. 3: The decision boundaries trained by (left) PUAL and (right) GLLC on the synthetic data with $\mathbf{mean}_{p_2} = 50, 100, 500$. Pink area: the negative region of PUAL; orange area: the negative region of GLLC; red points: positive instances; blue points: negative instances; the instances in the plots are from the test sets.

4.2.1 Real-World Datasets

Firstly, 16 datasets from the UCI Machine Learning Repository (<https://archive.ics.uci.edu/ml/index.php>) were selected to assess the performance of PUAL and verify our motivation: Accelerometer (**Acc**), **Ecoli**, Pen-Based Recognition of Handwritten Digits (**Pen**), Online Retail (**OR1**), Online Retail II (**OR2**), Parking Birmingham (**PB**), **wifi**, Sepsis survival minimal clinical records (**SSMCR**), Avila, Raisin Dataset (**RD**), Occupancy Detection (**OD**), User Knowledge Modeling Data Set (**UMD**), **Seeds**, Energy efficiency Data Set (**ENB**), Heart Disease (**HD**) and Liver Disorders (**LD**). The details of these real-world datasets are summarized in Table 2.

Table 2: Summary of the real-world datasets.

Dataset	Positive instances	Negative instances	# Features
Acc	100 red	100 blue	4
Ecoli	116 im & 52 pp	143 cp & 25 om	6
Pen	200 one & 200 eight	400 four	16
OR1	301 UK	301 Germany	4
OR2	500 UK	500 Germany	4
SSMCR	391 alive	109 dead	3
PB	500 Bull Ring	500 BHMBCCMKT01	3
OD	100 occupied	300 not occupied	5
UMD	83 Low	63 high	5
Seeds	70 Kama	70 Rosa	7
ENB	144 TypeII	144 Type III	7
wifi	100 Location 2& 100 Location 4	499 Location 1 & 100 Location 3	7
Avila	300 E	900 A	10
RD	450 Kecimen	450 Besni	7
LD	144 class 1	200 class 2	6
HD	150 absence	119 presence	13

4.2.2 Compared Methods

GLLC, uPU and nnPU were also trained on the 16 real datasets as the compared methods with PUAL. GLLC serves as the baseline of PUAL. uPU and nnPU are two consistent PU learning methods.

4.2.3 Training-Test Split for the Real PU Datasets

Different from the steps in Section 4.1.2, PU training and test sets for the 16 real datasets are constructed under the case-control scenario since we would like to see the performance of PUAL on the datasets with various labeling mechanism. Furthermore, under the case-control scenario, it is possible to do fair comparison between GLLC and the two convincing methods for PU classification, i.e., uPU [19] and nnPU [20], since they were proposed under the case-control scenario. The steps to perform training-test split for the 16 PU real datasets are summarized as follows:

1. To obtain the binary positive-negative (PN) datasets from the original multi-class dataset, certain classes in each of the original real datasets were treated as positive while some other classes were treated as negative with the rest of classes abandoned.
2. To construct the labeled-positive set and unlabeled-set, γ' of the positive instances in each binary PN dataset obtained in Step 1 were randomly selected to form the labeled-positive set, and the rest of the positive instances were mixed into the unlabeled set, contributing to the unlabeled set of the PU dataset.
3. To generate the training set and the test set from the constructed PU datasets, the labeled-positive set and 70% of the instances in the unlabeled set were selected as the training set while the test set was constituted by the rest 30% of the instances in the unlabeled set; this corresponds to the setting of case-control scenario since the unlabeled training set and the test set can be regarded to be sampled from the same population.

During preliminary experiments, we found that the label frequency γ needs to be greater than 20% for the hyper-parameter tuning strategy introduced in Section 4.2.4 to achieve adequate results. Therefore, the value of γ' is set to $\frac{7}{17}, \frac{7}{37}$ so that we have the label frequency $\gamma = \gamma' / (0.3\gamma' + 0.7) = 0.5, 0.25$, which is the fraction of positive instances that are labeled, in the corresponding constructed PU training sets, respectively. Then Step 2 and Step 3 were repeated for 10 times on each of the 16 binary PN datasets and obtained 10 pairs of PU training and test sets for each of the 16 binary PN datasets with a certain value of γ' .

4.2.4 Model Setting

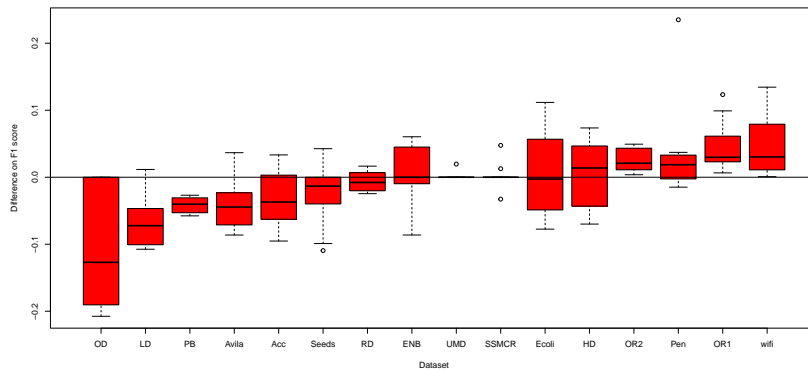
At the case-control scenario, we also use PUF-score in Equation (31) for hyper-parameter selection. The numerator ‘recall’ can still be estimated by computing $\frac{1}{n_p} \sum_{\mathbf{x}_i \in X_{[p]}} \mathbb{I}(\text{sgn}(f(\mathbf{x}_i)) = 1)$, while the denominator $P[\text{sgn}(f(\mathbf{x})) = 1]$ needs to be estimated by computing $\frac{1}{n_u} \sum_{\mathbf{x}_i \in X_{[u]}} \mathbb{I}(\text{sgn}(f(\mathbf{x}_i)) = 1)$ at the case-control scenario. Therefore, by fixing C_p to 1 and the number K of the nearest neighbors to 5, C_u, λ, σ in the objective functions of PUAL and GLLC were firstly tuned by 4-fold CV, which reached the highest average PUF-score.

Furthermore, considering the higher complexity of the real datasets compared with the synthetic datasets in Section 4.1, we modified our strategy for hyper-parameter selection, enabling efficient selection of hyper-parameters across a broader range. More specifically, λ, σ were tuned from the set $\{10^{-4}, 10^{-3}, 10^{-2}, 10^{-1}, 10^0, 10^1, 10^2, 10^3, 10^4\}$ and C_u was selected to from the set $\{0.5, 0.3, 0.1, 0.05, 0.01\}$ based on the setting in [26]. Then λ, σ and C_u were continually tuned following the greedy algorithm based on the average PUF-score on the validation sets as follows:

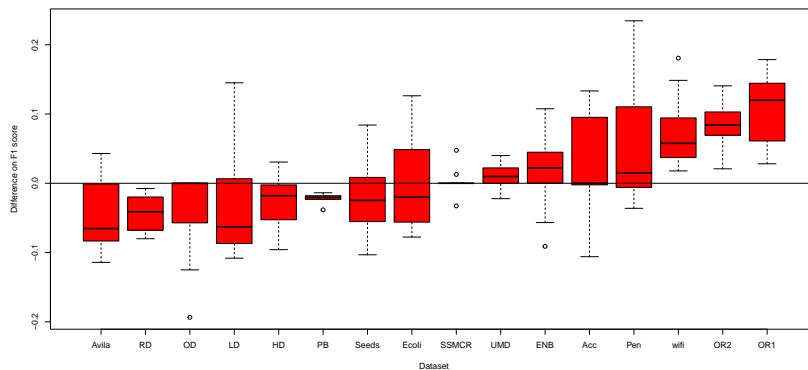
1. Set λ, σ and C_u to the best combination from the grid search.
2. Sequentially update one of hyper-parameters λ, σ and C_u by increasing/decreasing 10% of its current value with the rest of the hyper-parameters unchanged. The optimal scenario on 4-fold CV is set to be the final update of this step.
3. Repeat Step 2 until there is no better scenario appearing.

In addition, the hyper-parameters of uPU and mnPU were fixed as the recommended setting in the open source provided by [20] at <https://github.com/kiriyor/mnPUlearning>. Radial Basis Function (RBF) kernel was applied to both PUAL and GLLC. More specifically, we computed $\exp(-\|x_i - x_j\|^2/2\lambda^2)$ as the (i, j) element of $\Phi'(\phi(\mathbf{X}_{[pu]}), \phi(\mathbf{X}_{[pu]}))$.

4.2.5 Summary of Comparison between PUAL and GLLC



(a) $\gamma = 0.5$



(b) $\gamma = 0.25$

Fig. 4: Boxplots for the difference between F1-scores of PUAL and GLLC on each dataset increasingly ranked by medians; label frequencies $\gamma = 0.5$ (top) and 0.25 (bottom); x-axis: the datasets; y-axis: the difference between PUAL and GLLC in F1-score.

The results of the difference between the F1-scores of PUAL and GLLC on each pairwise experiments are shown in the boxplots in Fig. 4 with $\gamma = 0.5, 0.25$, respectively. In both figures, the best four datasets for PUAL over GLLC are **wifi**, **OR1**, **OR2**, and **Pen**. Furthermore, with $\gamma = 0.5, 0.25$, three of the worst four datasets for PUAL compared with GLLC are **OD**, **LD**, **Avila**. When $\gamma = 0.5$, the rest one of the worst four datasets is **PB**; when $\gamma = 0.25$, it is **RD**. According to the t-tests with p -value lower than 0.05 between the pairwise results of these four methods, there are totally 8 cases where PUAL is the optimal choice among the four methods.

4.2.6 Pattern Analysis for the Real Datasets Preferring PUAL to GLLC

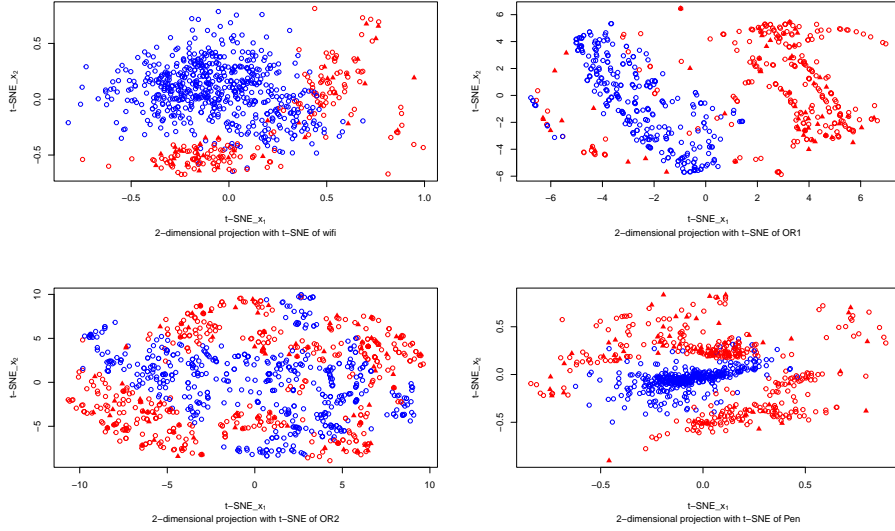


Fig. 5: The t-SNE plots of the best four datasets **wifi**, **OR1**, **OR2** and **Pen**; the perplexity for the training of t-SNE on these four datasets was set to 750, 40, 250, 750, respectively; label frequency $\gamma=0.25$; red: positive instances; blue: negative instances; triangle: labeled instances; circle: unlabeled instances.

The t-SNE plots of the best four datasets, i.e., **wifi**, **OR1**, **OR2**, and **Pen**, for PUAL compared with GLLC are shown in Fig. 5. According to the four t-SNE plots, the following observations can be made:

1. The trifurcate pattern of the best four datasets in Fig. 5 is clear that the positive set is constituted by two subsets distributing on both sides of the negative set as discussed in the motivation of PUAL in Section 3.1.
2. In the t-SNE plot of dataset **OR1**, there are many more instances in the right-hand labeled-positive subset than the instances in the left-hand labeled-positive set. This

indicates that the trifurcate pattern does not have to be balanced for PUAL to outperform GLLC.

4.2.7 Pattern Analysis for the Real Datasets Preferring GLLC to PUAL

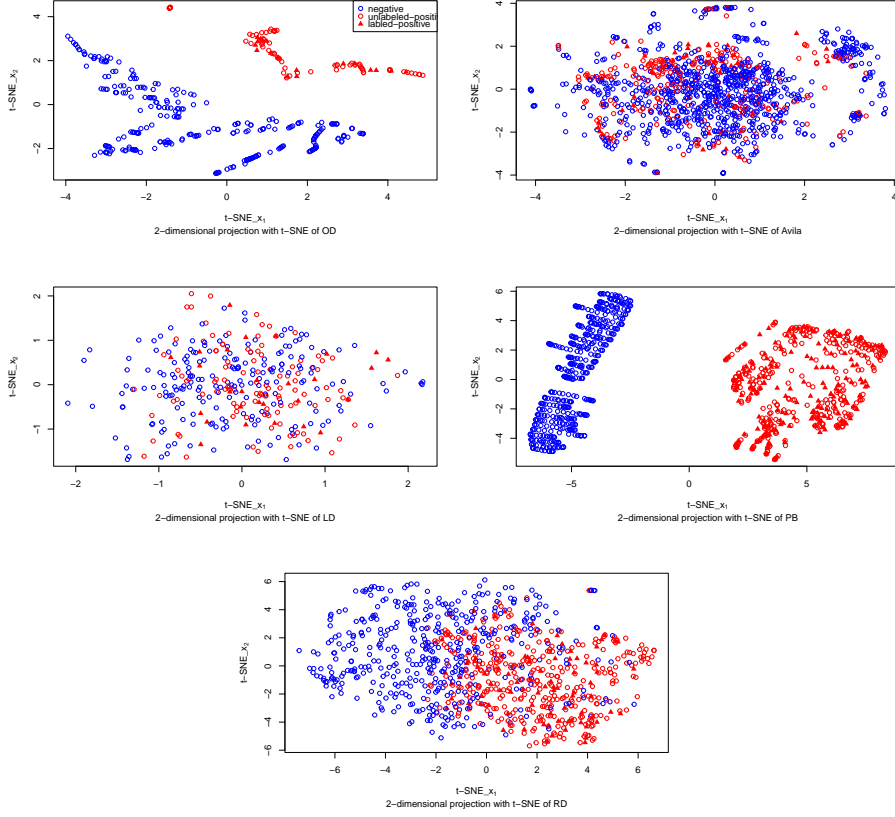


Fig. 6: The t-SNE plots of the worst five datasets **OD**, **Avila**, **LD**, **PB**, **RD**; cross entropy loss for training with perplexity = 200, 550, 250, 300, 300; label frequency $\gamma=0.25, 0.25, 0.25, 0.5, 0.25$. The rest of the caption is as in Fig. 5.

There are overall five datasets to be the worst four datasets for PUAL compared with GLLC under two cases of label frequency, i.e., $\gamma = 0.5, 0.25$. The t-SNE plots for them are illustrated in Fig. 6 and their patterns can be summarized as follows:

1. According to the t-SNE plots of the two datasets **LD** and **Avila**, the positive set and the negative set are mixed together, making the dataset challenging to be separated. In this case, the labeled-positive instances selected as support vectors

by the hinge loss of PUAL are not sufficient to adequately represent the pattern of the positive set, while the squared loss of GLLC on the labeled-positive set, which selects all positive instances as the support vectors, can somewhat alleviate this issue. As a result, GLLC on these two datasets outperforms PUAL.

2. The t-SNE plots of the three datasets **OD**, **PB**, and **RD** represent the typical two-class patterns. In this type of datasets, the problem of GLLC mentioned in Section 3.1 does not exist. Therefore, the optimal combination(s) of the hyper-parameters for GLLC to outperform PUAL was (were) found in at least one case of label frequency γ .

4.2.8 Comparison between PUAL, uPU and nnPU

The performance of PUAL, GLLC, uPU and nnPU on the 16 real datasets are summarized in Table 3, from which we can obtain the following findings. First, there are in total 22 cases of the 32 cases where PUAL outperforms uPU and nnPU. Secondly, uPU and nnPU sometimes have much larger standard deviations than PUAL since their algorithms based on Adam for the optimization of their non-convex objective functions cannot always converge to the optimal solution, although nnPU alleviates this issue to some extent.

Table 3: The average F1-score (%) of the classifiers. For each of the 16 original datasets, the average F1-scores and standard deviations in the two rows were obtained under label frequencies $\gamma = 0.5$ (top) and 0.25 (bottom), respectively. In each row, the result highlighted in blue indicates the statistically optimal choice among the four methods according to the t-tests with p -value lower than 0.05 (Sometimes an optimal choice was missed in a row since there was no such a method holding statistically significantly higher F1-score than other methods).

Dataset	PUAL	GLLC	uPU	nnPU
ENB	42.82 \pm 4.76	42.69 \pm 4.62	29.58 \pm 22.14	30.20 \pm 23.67
	45.82 \pm 7.50	44.16 \pm 6.56	26.12 \pm 30.53	26.88 \pm 31.28
HD	82.72 \pm 2.35	81.97 \pm 5.45	71.38 \pm 4.23	74.38 \pm 2.19
	81.92 \pm 4.03	84.46 \pm 4.11	71.01 \pm 3.97	75.06 \pm 2.40
Pen	92.47 \pm 8.13	88.92 \pm 10.15	77.76 \pm 31.00	87.50 \pm 14.94
	91.73 \pm 9.04	87.02 \pm 11.38	72.55 \pm 31.03	84.06 \pm 16.85
LD	44.24 \pm 5.72	50.79 \pm 6.86	11.88 \pm 25.75	31.54 \pm 27.79
	36.85 \pm 9.97	40.05 \pm 8.85	10.15 \pm 22.39	20.09 \pm 26.27
OR1	90.05 \pm 2.25	85.62 \pm 3.77	16.64 \pm 33.33	84.08 \pm 6.88
	83.88 \pm 5.78	72.95 \pm 5.50	20.90 \pm 33.12	72.06 \pm 6.99
RD	82.45 \pm 2.18	83.01 \pm 2.38	70.61 \pm 12.89	71.29 \pm 13.63
	77.63 \pm 3.77	81.99 \pm 2.84	72.92 \pm 14.53	73.12 \pm 12.83
Seeds	92.31 \pm 4.86	94.63 \pm 2.81	92.37 \pm 1.51	97.25 \pm 3.65
	89.05 \pm 5.53	91.18 \pm 4.48	86.85 \pm 3.12	93.08 \pm 3.89
wifi	95.10 \pm 1.96	90.43 \pm 4.65	91.16 \pm 4.29	92.17 \pm 3.17
	96.69 \pm 1.83	89.09 \pm 4.77	87.69 \pm 2.88	89.27 \pm 2.61
Avila	55.82 \pm 2.90	59.56 \pm 4.10	62.74 \pm 8.82	63.75 \pm 9.07
	50.05 \pm 4.22	54.99 \pm 6.17	61.30 \pm 9.23	61.00 \pm 9.04

Table 3 – continued from previous page

Dataset	PUAL	GLLC	uPU	nnPU
OD	89.00 ± 8.44	100.00 ± 0.00	80.00 ± 42.16	100.00 ± 0.00
	95.69 ± 6.74	100.00 ± 0.00	80.00 ± 42.16	100.00 ± 0.00
OR2	88.93 ± 1.22	86.49 ± 1.38	76.92 ± 4.90	81.60 ± 4.23
	85.50 ± 3.42	77.10 ± 5.65	74.41 ± 5.45	77.28 ± 3.76
PB	95.90 ± 1.12	100.00 ± 0.00	69.77 ± 2.62	67.19 ± 3.17
	97.86 ± 0.67	100.00 ± 0.00	68.75 ± 2.63	66.63 ± 4.09
Acc	65.02 ± 4.79	68.10 ± 2.18	20.05 ± 27.57	20.46 ± 28.56
	66.36 ± 4.42	64.08 ± 6.31	21.95 ± 29.61	23.43 ± 31.40
Ecoli	90.80 ± 2.59	90.15 ± 6.28	84.41 ± 6.13	85.92 ± 6.69
	88.04 ± 4.44	88.03 ± 3.96	84.92 ± 6.82	86.05 ± 6.55
SSMCR	87.63 ± 1.29	87.35 ± 2.14	85.71 ± 1.98	87.42 ± 1.37
	87.63 ± 1.29	87.35 ± 2.14	84.97 ± 2.03	86.79 ± 1.50
UMD	100.00 ± 0.00	99.80 ± 0.62	100.00 ± 0.00	100.00 ± 0.00
	99.58 ± 0.88	98.41 ± 1.80	100.00 ± 0.00	100.00 ± 0.00

5 Conclusion

In this paper, we propose PUAL for better classification on trifurcate PU datasets, where the positive set is constituted by two subsets distributing on both sides of the negative set. The key novelty of PUAL is an asymmetric structure composed of hinge loss and squared loss for training the PU classifier. Experimental results demonstrate the superiority of PUAL in performing PU classification on trifurcate data. As an SVM-based method, PUAL is still negatively affected by the irrelevant features in the datasets, partly due to the L2 regularization term of model parameters, which cannot compress the coefficients of the irrelevant features to be exactly zero thoroughly [42]. To address this issue, a future work is to explore the L1 regularization term of the model parameters for PUAL.

References

- [1] Ren, Y., Ji, D., Zhang, H.: Positive unlabeled learning for deceptive reviews detection. In: Proceedings of the 2014 Conference on Empirical Methods in Natural Language Processing (EMNLP), pp. 488–498 (2014)
- [2] Li, H., Chen, Z., Liu, B., Wei, X., Shao, J.: Spotting fake reviews via collective positive-unlabeled learning. In: 2014 IEEE International Conference on Data Mining, pp. 899–904 (2014). IEEE
- [3] Li, W., Guo, Q., Elkan, C.: A positive and unlabeled learning algorithm for one-class classification of remote-sensing data. IEEE transactions on geoscience and remote sensing **49**(2), 717–725 (2010)
- [4] Dai, S., Li, X., Zhou, Y., Ye, X., Liu, T.: GradPU: positive-unlabeled learning via gradient penalty and positive upweighting. In: Proceedings of the AAAI Conference on Artificial Intelligence, vol. 37, pp. 7296–7303 (2023)

- [5] Liu, B., Lee, W.S., Yu, P.S., Li, X.: Partially supervised classification of text documents. In: ICML, vol. 2, pp. 387–394 (2002). Sydney, NSW
- [6] Yu, H., Han, J., Chang, K.-C.: PEBL: Web page classification without negative examples. *IEEE Transactions on Knowledge and Data Engineering* **16**(1), 70–81 (2004)
- [7] Li, X., Liu, B.: Learning to classify texts using positive and unlabeled data. In: IJCAI, vol. 3, pp. 587–592 (2003)
- [8] He, F., Liu, T., Webb, G.I., Tao, D.: Instance-dependent PU learning by Bayesian optimal relabeling. arXiv preprint arXiv:1808.02180 (2018)
- [9] Liu, B., Liu, Z., Xiao, Y.: A new dictionary-based positive and unlabeled learning method. *Applied Intelligence*, 1–15 (2021)
- [10] Liu, B., Liu, Q., Xiao, Y.: A new method for positive and unlabeled learning with privileged information. *Applied Intelligence* **52**(3), 2465–2479 (2022)
- [11] Ienco, D., Pensa, R.G., Meo, R.: From context to distance: Learning dissimilarity for categorical data clustering. *ACM Transactions on Knowledge Discovery from Data (TKDD)* **6**(1), 1–25 (2012)
- [12] Liu, L., Peng, T.: Clustering-based Method for Positive and Unlabeled Text Categorization Enhanced by Improved TFIDF. *Journal of Information Science & Engineering* **30**(5) (2014)
- [13] Chaudhari, S., Shevade, S.: Learning from positive and unlabelled examples using maximum margin clustering. In: *International Conference on Neural Information Processing*, pp. 465–473 (2012). Springer
- [14] Ke, T., Yang, B., Zhen, L., Tan, J., Li, Y., Jing, L.: Building high-performance classifiers using positive and unlabeled examples for text classification. In: *International Symposium on Neural Networks*, pp. 187–195 (2012). Springer
- [15] He, Y., Li, X., Zhang, M., Fournier-Viger, P., Huang, J.Z., Salloum, S.: A novel observation points-based positive-unlabeled learning algorithm. *CAAI Transactions on Intelligence Technology* **8**(4), 1425–1443 (2023)
- [16] Xu, C., Liu, C., Yang, S., Wang, Y., Zhang, S., Jia, L., Fu, Y.: Split-PU: Hardness-aware Training Strategy for Positive-Unlabeled Learning. In: *Proceedings of the 30th ACM International Conference on Multimedia*, pp. 2719–2729 (2022)
- [17] Dorigatti, E., Goschenhofer, J., Schubert, B., Rezaei, M., Bischl, B.: Positive-Unlabeled Learning with Uncertainty-aware Pseudo-label Selection. arXiv preprint arXiv:2201.13192 (2022)
- [18] Liang, Q., Zhu, M., Wang, Y., Wang, X., Zhao, W., Yang, M., Wei, H., Han, B.,

- Zheng, X.: Positive distribution pollution: rethinking positive unlabeled learning from a unified perspective. In: Proceedings of the AAAI Conference on Artificial Intelligence, vol. 37, pp. 8737–8745 (2023)
- [19] Du Plessis, M.C., Niu, G., Sugiyama, M.: Analysis of learning from positive and unlabeled data. *Advances in neural information processing systems* **27** (2014)
- [20] Kiryo, R., Niu, G., Plessis, M.C.d., Sugiyama, M.: Positive-unlabeled learning with non-negative risk estimator. *arXiv preprint arXiv:1703.00593* (2017)
- [21] Su, G., Chen, W., Xu, M.: Positive-unlabeled learning from imbalanced data. In: Proceedings of the 30th International Joint Conference on Artificial Intelligence, Virtual Event (2021)
- [22] Liu, B., Dai, Y., Li, X., Lee, W.S., Yu, P.S.: Building text classifiers using positive and unlabeled examples. In: Third IEEE International Conference on Data Mining, pp. 179–186 (2003). IEEE
- [23] Cortes, C., Vapnik, V.: Support vector machine. *Machine learning* **20**(3), 273–297 (1995)
- [24] Liu, Z., Shi, W., Li, D., Qin, Q.: Partially supervised classification: based on weighted unlabeled samples support vector machine. In: Data Warehousing and Mining: Concepts, Methodologies, Tools, and Applications, pp. 1216–1230 (2008)
- [25] Ke, T., Lv, H., Sun, M., Zhang, L.: A biased least squares support vector machine based on Mahalanobis distance for PU learning. *Physica A: Statistical Mechanics and its Applications* **509**, 422–438 (2018)
- [26] Ke, T., Jing, L., Lv, H., Zhang, L., Hu, Y.: Global and local learning from positive and unlabeled examples. *Applied Intelligence* **48**(8), 2373–2392 (2018)
- [27] Gong, C., Liu, T., Yang, J., Tao, D.: Large-margin label-calibrated support vector machines for positive and unlabeled learning. *IEEE transactions on neural networks and learning systems* **30**(11), 3471–3483 (2019)
- [28] Maaten, L.: Visualizing data using t-SNE. *Journal of machine learning research* **9**(Nov), 2579 (2008)
- [29] Bhatt, R.: Wireless Indoor Localization. UCI Machine Learning Repository. DOI: <https://doi.org/10.24432/C51880> (2017)
- [30] Scott, C., Blanchard, G.: Novelty detection: Unlabeled data definitely help. In: Artificial Intelligence and Statistics, pp. 464–471 (2009). PMLR
- [31] Chapelle, O., Scholkopf, B., Zien, A.: Semi-supervised learning (chapelle, o. et al., eds.; 2006)[book reviews]. *IEEE Transactions on Neural Networks* **20**(3), 542–542 (2009)

- [32] Gabay, D., Mercier, B.: A dual algorithm for the solution of nonlinear variational problems via finite element approximation. *Computers & mathematics with applications* **2**(1), 17–40 (1976)
- [33] Boyd, S., Parikh, N., Chu, E., Peleato, B., Eckstein, J.: Distributed optimization and statistical learning via the alternating direction method of multipliers. *Foundations and Trends® in Machine learning* **3**(1), 1–122 (2011)
- [34] Ye, G.-B., Xie, X.: Split Bregman method for large scale fused Lasso. *Computational Statistics & Data Analysis* **55**(4), 1552–1569 (2011)
- [35] Jain, S., White, M., Trosset, M.W., Radivojac, P.: Nonparametric semi-supervised learning of class proportions. *arXiv preprint arXiv:1601.01944* (2016)
- [36] Christoffel, M., Niu, G., Sugiyama, M.: Class-prior estimation for learning from positive and unlabeled data. In: *Asian Conference on Machine Learning*, pp. 221–236 (2016). PMLR
- [37] Bekker, J., Davis, J.: Estimating the class prior in positive and unlabeled data through decision tree induction. In: *Proceedings of the AAAI Conference on Artificial Intelligence*, vol. 32 (2018)
- [38] Genton, M.G.: Classes of kernels for machine learning: a statistics perspective. *Journal of machine learning research* **2**(Dec), 299–312 (2001)
- [39] Bekker, J., Davis, J.: Learning from positive and unlabeled data: a survey. *Mach. Learn.* **109**(4), 719–760 (2020)
- [40] Lee, W.S., Liu, B.: Learning with positive and unlabeled examples using weighted logistic regression. In: *ICML*, vol. 3, pp. 448–455 (2003)
- [41] Liu, Y., Zhao, J., Xu, Y.: Robust and unbiased positive and unlabeled learning. *Knowledge-Based Systems* **277**, 110819 (2023)
- [42] Nguyen, H.T., Franke, K., Petrović, S.: On general definition of L1-norm support vector machines for feature selection. *International Journal of Machine Learning and Computing* **1**(3), 279 (2011)